MASTER THESIS

AUGMENTING AN EMG-DRIVEN MUSCULOSKELETAL MODEL BY ACCOUNTING FOR INTRINSIC MUSCLE PROPERTIES TO IMPROVE JOINT STIFFNESS ESTIMATION

Maria João Cabral

FACULTY OF ENGINEERING TECHNOLOGY
DEPARTMENT OF BIOMECHANICAL ENGINEERING

EXAMINATION COMMITTEE
prof. dr. ir H. van der Kooij
prof. dr. ir J.H. Buurke
ir. C.P. Cop
dr. ir. M. Sartori

DOCUMENT NUMBER
BW - 667

UNIVERSITY OF TWENTE.

10-07-2019

Augmenting an EMG-driven musculoskeletal model by accounting for intrinsic muscle properties to improve joint stiffness estimation

Maria João Cabral[1], Pablo Cop[1] and Massimo Sartori[1]

Objective: Short-range stiffness (SRS) is the main muscle mechanism to respond to perturbations. In current literature no models of SRS have been applied to dynamic tasks. In this study, a novel methodology to implement SRS in electromyography(EMG)-driven musculoskeletal modeling and further validation in dynamic and static tasks against system identification techniques is proposed. Methods: EMG signals, motion capture, and kinematic and dynamic data of the ankle joint and surrounding muscle acquired during plantar-dorsi flexion movements were used used to drive the musculoskeletal modelling framework in order to estimate ankle joint stiffness. A model of SRS was added to the modeling framework. An automatic fiber stretch detection algorithm was developed to trigger SRS. An optimization algorithm was implemented to account for amplitude of the movement in SRS calculation. Results: The proposed model with the inclusion of SRS improved the estimations of joint stiffness in comparison with the model without SRS, especially during the static conditions. The model was able to differentiate between the different tasks, by increasing or decreasing the contribution of SRS when the muscles suffered large or small amplitude of movement, respectively. The model detected with an accuracy of 92% the perturbations applied and, consequently, the trigger of SRS. Conclusion: The suggested methodology provides a prof of concept to implement SRS in musculoskeletal models. The ability to trigger the computation of SRS without providing additional information to the model and adjusting the computed SRS according to the amplitude of the movement enables the application of the model in any type of task.

I. INTRODUCTION

Human movement results from the response of the muscles to afferent and efferent neuronal stimuli. Although the mechanisms used during movement are very complex, most of them occur at a subconscious level, so no mental effort is required (Ogawa et al. 2013). This is the case of the adaptation to different environmental conditions, different terrains or external perturbations. The central nervous system is largely responsible for the innervation of the muscle fibres that will evoke a certain viscoelastic response in the muscle, leading to a modulation of the viscoelastic response at the joint level, i.e. joint stiffness (Winter 2009; Latash and Zatsiorsky 1993). Stiffness is a term widely used in the mechanical engineering field to describe the resistance that a body offers to deformation when a force is applied (Winter 2009). The concept of joint stiffness is, therefore, very controversial since a joint is not a single body, but a combination of multiple bodies with different elastic responses (Latash and Zatsiorsky 1993). Here, we define joint stiffness as the combination of the elastic response of the biologic tissues that surround the joint. In some neuron-motor diseases, e.g. cerebral palsy, joint stiffness is impaired resulting in uncoordinated movement, weak and stiff muscles and tremors. Cerebral palsy is a movement disorder that appears early in childhood and it occurs in about 2.1 per 1,000 live births (Oskoui et al. 2013), being the most common movement disorder in childhood. Understanding the muscle strategies that modulate joint stiffness and translating this knowledge into technological solutions will allow provision of more personalized rehabilitation treatments (Ogawa et al. 2013), development of biomimetic prostheses (Sartori, Lloyd, and Farina 2016) and improvement of clinical assessments for neural-motor diseases (de Groote, Blum, et al. 2018; Eggleston, Harry, and Dufek 2018; Galli et al. 2018).

[1] Biomechanics Department, Biomedical Engineering University of Twente, 7500 AE Enschede, The Netherlands

The neural modulation of viscoelastic properties of the joints started to be questioned in some conditions, when in experimental measurements very large values of tension were measured for the very early stretch of the muscle fibre after isometric contraction (Joyce, P. Rack, and Westbury 1969). Joyce explained these findings through the sliding filament theory of muscle contraction, more specifically through the rate of formation and deformation of the cross-bridges between the thick and the thin filaments within the myofibrils. At high stimulation rates, there would be a strong tendency to form cross-links, so during lengthening a higher number of cross-bridges will stretch or deform originating an increase of force exerted. At lower stimulation rates, the cross-links would be formed more slowly, so by moving the filaments the rate of deformation of the cross-links would increase leading to a fall in tension (Joyce, P. Rack, and Westbury 1969). A later study deeply investigated the behaviour of muscles during different velocities and amplitudes of movement, confirming the steep rise in tension for the first distance of stretch and the increase in steepness with higher stimulation rates (P. M. Rack and Westbury 1974). The force in the muscle rises in two phases with the stretch of the fiber: an initial rapid increase over a small stretch (short-range regime), and a slower and more modest rise over the remainder of the stretch (complaint regime) (Getz, Cooke, and Lehman 1998).

The term short-range stiffness (SRS) originated to represent the intrinsic property of muscle fibres, resulting from the force produced by the muscle while stretching due to distortion, but not breakage, of the cross-bridges between the thin and thick filaments within the myofibrils (P. M. Rack and Westbury 1974). This muscle property is independent on the velocity of the movement but varies with the tension in the fibre and with the amplitude of the movement (P. M. Rack and Westbury 1974). The only dependency with velocity of the movement observed was with respect to the duration of the short-range regime, but not the magnitude of the SRS (P. M. Rack and Westbury 1974). Aside from the fibre stretch dependency, more recent studies have shown that SRS is also a time-dependent feature of muscle contraction (van Eesbeek et al. 2010; de Vlugt et al. 2011). The concept of initial mechanical response arose to describe the first 50 ms after a perturbation, in which no change in muscle activity due to spinal reflexes occurs, so changes in muscle force during this period can only be attributed to intrinsic muscle properties (de Groote, Allen, and Ting 2017). Although SRS is defined as a mechanical property of the muscle, it can clearly influence the biomechanics of the joint. Moreover, in tasks with small range of motion in which the fibers do not stretch beyond the elastic limit of the cross-bridges.

Joint stiffness has been widely estimated by system identification methods in conjugation with joint perturbation techniques in order to determine a relationship between joint angle and joint torque, in static or dynamic conditions (Rouse et al. 2013). An advantage of this method is that joint stiffness can be estimated without prior knowledge about the structures spanning the joint. However, the presence of external perturbations in the joint is always required, which is not always convenient, especially in pathological situations were simple movements are already very demanding for the patient.

In order to overcome this issue, in the last decade more effort has been put into developing musculoskeletal models that can estimate joint stiffness in static (Hu, Murray, and Perreault 2011; Pfeifer et al. 2012) and dynamic (Sartori, Maculan, et al. 2015) conditions. A musculoskeletal model uses kinematic data and measured moments and forces to compute joint angles and moments through inverse kinematic and dynamic approaches. Due to muscle redundancy most of the musculoskeletal models use an optimization algorithm to find a unique solution (Delp et al. 2007). To provide a more physiological solution to this problem, musculoskeletal models that also include electromyography (EMG) recordings to obtain an unique solution were developed (Sartori, Maculan, et al. 2015). Recorded EMG signals and kinematic data are used to compute muscle activations and muscle fiber lengths and moments arms of a certain number of muscle tendon units (MTUs). Muscle dynamics are computed based on the equations of the Hill-type muscle model. Then, the dynamic response of each MTU is projected into the joint level in order to obtain joint moments. During calibration, the model runs in a closed loop until it calibrates the subject-specific parameters by minimizing the difference between the reference torque and the estimated torque. After calibration, the model works in open loop and does not require reference torques. An advantage of this method is the calculation of the individual contribution of each muscle to the global joint stiffness, so co-contraction strategies can be taken into account. The framework proposed by (Sartori, Maculan, et al. 2015) was validated in perturbed sinusoidal dynamic and static conditions of the ankle joint against system identification techniques (Cop et al. 2019). The model estimated joint stiffness sufficiently well for fast dynamic tasks, but for slow dynamic movement and static conditions the model underestimated the global joint stiffness.

To drive any musculoskeletal model a mathematical representation of the viscoelastic response of the muscle and the surrounding biological tissues is required. Most of the modeling approaches found in literature use a Hill-type muscle model to compute the muscle-tendon properties. The standard Hill-type muscle model used is composed of three components: an active contractile element, a passive parallel element and a series element. The active contractile element models the active force generated by the sliding filaments at the sarcomere level. The passive parallel element represents the force of the connective tissues surrounding the contractile element. The series element represents the tendon (Hill 1938). In this model, the intrinsic properties of the muscle, such as short-range stiffness and history-dependency muscle properties are not taken into account (Martins et al. 1998; McGowan, Neptune, and Herzog 2013). As discussed previously these properties can have a crucial role in the modulation of joint stiffness in adaptation to external stimuli. Therefore, we consider that our EMG-driven musculoskeletal model underestimated the global joint stiffness for static conditions probably due to the absence of the intrinsic muscle properties in the modeling framework.

Several research groups have attempted to include SRS in musculoskeletal models. A common assumption across all approaches consists of allocating SRS in the contractile element of the Hill-type muscle model (Loram, Maganaris, and Martin Lakie 2007). SRS was modelled in static postures of the arm for the calculation of instantaneous endpoint stiffness (Hu, Murray, and Perreault 2011). In this study, SRS was proportional to the initial isometric force in each muscle in series with the stiffness of the tendon, the same approach tested previously in felines (Cui et al. 2008). The results showed that SRS is a crucial mechanism in the estimation of end point stiffness. However, this method was only applied within the conditions of short-range stiffness, i.e. while the muscle fibres are not stretched beyond the short-range regime. Another study developed a model to compute SRS at the joint level during imposed wrist rotations (de Vlugt et al. 2011). Here, SRS was modelled with a dynamic nonlinear model, in which a transitioning behavior between the short-range regime and the more compliant regime was included based on the joint angle. However, the model was only applied in static conditions, and, additionally, no discrimination between individual muscle contributions was made. So far, there was no model that accounted for the stretch limit of the muscle fibers and, therefore, it has not been possible to implement it for dynamic tasks.

A recent study published by De Groote et al., approached this problem by developing a dynamic model of muscle short-range stiffness to augment a Hill-type muscle model (de Groote, Allen, and Ting 2017). The model was applied during the initial mechanical response to perturbed standing position and the ankle, knee and hip joint torques were computed. The SRS force in the muscle was modelled proportional to the isometric force prior to the perturbation, as reported by (Cui et al. 2008), but a fibre stretch dependency was added to the model in order to adapt it to dynamic tasks. The results showed that short-range stiffness is an important consideration in simulations of perturbed movements (de Groote, Allen, and Ting 2017). Even though this study has shown great results at the torque level, no computation of the joint stiffness has been done. Moreover, this model was implemented with a clear starting point to trigger SRS, which means that it cannot be applied in continuous tasks.

In the present study, an extension of the SRS model suggested by De Groote et al. (2017) is implemented into the EMG-driven musculoskeletal model developed by Sartori, Maculan, et al. 2015, in order to better estimate ankle joint stiffness in perturbed dynamic and static tasks. To assess the contribution of short-range stiffness to the estimation of joint stiffness during dynamic tasks, we first modelled SRS by augmenting the Hill-type muscle model and included it in the EMG-driven musculoskeletal model developed by Sartori, Maculan, et al. 2015. Secondly, we created a model to determine when SRS should be triggered. Using the fiber acceleration profile the model is able to automatically transition from the compliant regime to the short-range regime of the muscle fiber. Finally, we implemented an optimization algorithm which accounts for the amplitude of the movement of each muscle fiber. We hypothesize that including SRS as a muscle property in the EMG-driven musculoskeletal model will improve the prediction of joint stiffness, especially during static conditions. Additionally, having a method to automatically trigger the short-range regime will widen the applicability of these frameworks into biomimetic prostheses, that can further be applied in rehabilitation of neuromotor disorders.

II. METHODS

The proposed framework was applied to the data set recorded in a previous study (Cop et al. 2019) and the computed joint stiffness was validated against system identification techniques which were performed by yet another study (Moya Esteban et al. 2019). For more information on the experimental protocol (Section II - A), the EMG-musculoskeletal model (Section II - B) (Sartori, Maculan, et al. 2015) and the method used for system identification the reader is referred to the studies cited above.

A. Data Set

Six healthy subjects (age: 24.2 $\pm$ 1.0 years; weight: 68.8 $\pm$ 5.6 kg; height: 1.75 $\pm$ 0.08 m) participated in this study. The Achilles Rehabilitation Device (MOOG, Nieuw-Vennep, The Netherlands), an admittance controlled single axis manipulator, was used to measure the ankle joints position and torque. Motion capture data was acquired using a Visualeyez II tracker (PTI, Vancouver, Canada) at 100 Hz. EMG activity was recorded at 2048 Hz by the Porti system (TMSi, Oldenzaal, The Netherlands). The main parts of the experimental setup can be seen in Fig. 1. The experimental protocol consisted of two types of tasks, a dynamic and a static task. The Achilles Rehabilitation Device had a support for the foot and was able to mimic a selected viscoelastic environment to provide a certain resistance while it was moved. In dynamic tasks, subjects were asked to follow sinusoidal position targets (Fig. 1-II) with an amplitude of 0.15 rad at two different frequencies, 0.3 Hz (slow) and 0.6 Hz (fast), both in unperturbed and perturbed conditions. For these tasks, the viscoelastic environment of the Achilles device was characterized by a virtual inertia (i^v), damping (b^v), and stiffness (k^v) of 1 kg$\cdot m^2$, 2.5 N$\cdot$m$\cdot$s$\cdot rad^{-1}$, and 60 N$\cdot$m$\cdot$s$\cdot rad^{-1}$, respectively. In static tasks, the Achilles remained at a fixed position and subjects were asked to follow a sinusoidal torque target with an amplitude of 5 N$\cdot$m and a frequency of 0.8 Hz. The device was also able to provide pseudo-random perturbations at the ankle joint. These perturbations were set to apply random rotations of 0.03 rad at the ankle joint level. All tasks described before were tested in perturbed and unperturbed conditions. For all non perturbed conditions (No Pert) only one repetition was performed. For the perturbed conditions (Pert), for dynamic at 0.6Hz, dynamic at 0.3Hz and static tasks, six, eleven and four repetitions of each tasks were performed, respectively. The number of repetitions for each type of task was chosen in order to have approximately the same amount of plantar-dorsi flexion cycles. Each trial lasted 120 seconds. The order of the tasks, i.e. static, dynamic at 0.3Hz, and dynamic at 0.6Hz, was randomized across subjects to avoid bias due to the learning effects.

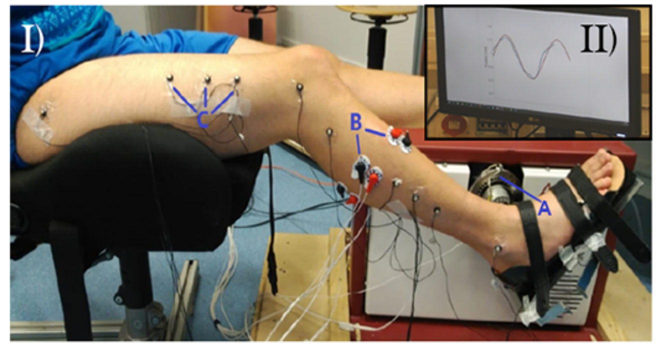

Fig. 1: I)Experimental setup. The Achilles Rehabilitation Device (A) was used to perturb and track the kinematics and dynamics of the ankle joint. Muscle activity (B) was recorded by the Porti system. Optical LED markers (C) were used to capture the knee and ankle angles. II) Screen in which the target (solid red line) and the subjects trajectory (solid blue line) are displayed.

The EMG data was acquired from five lower leg muscles: tibialis anterior, soleus, gastrocnemius medialis and lateralis, and peroneus longus. EMG signals were filtered and normalized by the value of maximum voluntary contraction (MVC) for each subject. For more details on the signal processing read Cop et al. 2019. Motion capture data was recorded using 12 optical markers placed on the subjects right leg.

Several bony landmarks were used for scaling the generic OpenSim Gait2392 Simbody anatomical model [1]. In addition to the markers on the bony landmarks ,three markers on the thigh and three markers on the shank were used to track the knee and ankle angles during the whole experiment. The measured position of the Achilles was recorded by the Porti and Visualeyez systems to perform off-line synchronization of the measurements of all devices used in the experiment.

B. EMG-driven musculoskeletal modeling framework

The EMG-driven musculoskeletal model is briefly explained here, for a more detailed description, the reader is referred to Sartori, Maculan, et al. 2015. As an input to the framework the properties of the each MTU such as activation, length, velocity and moment arm were calculated by the open-source toolbox Calibrated EMG-Informed Neuromusculoskeletal Modeling (CEINMS) [2] (Pizzolato et al. 2015) and by the open-source software OpenSim (Delp et al. 2007). The framework is composed of five different blocks:

- **A: MTU activation block.** The EMG signals recorded from five muscle groups are converted into activations (a(t)), which are used to drive seven MTUs. This means that the muscles that are not recorded from the EMG signals are obtained by mapping signals from other muscles. This is the case for the peroneus brevis and the tertius, whose activation patterns are obtained from the EMG signals of the peroneus longus and the tibialis anterior, respectively.
- **B: MTU kinematics block.** A generic model with seven MTUs and a single degree of freedom (DOF), i.e. ankle plantar-dorsi flexion, is adjusted to match the scaled OpenSim model. To estimate instantaneous MTU length l^{MTU} and MTU moment arm r as function of the ankle angle, two splines are created with the MTU length and moment arms obtained from the OpenSim as a function of the ankle angle.
- **C: MTU dynamics block.** Normalized generic force-velocity and force-length (both passive and active) curves are used in conjunction with $a(t)$, l^{MTU} and fiber velocity, v^{MTU}, obtained in previous blocks to compute MTU force, F^{MTU}. The force of the MTU is equal to the tendon force F^t. Since the tendon is in series with the muscle fibers, its force is the same to the muscle fibers force. The equation that is used corresponds to a Hill- type muscle model (Sartori, Maculan, et al. 2015).

$$F^{MTU} = F^t = F^m cos(\alpha) \tag{1}$$

The muscle stiffness K^m is estimated as the partial derivative of the muscle fiber force F^m with respect to the normalized muscle fiber length $\bar{l}^m$. The muscle force and muscle stiffness are modelled as two multi-dimensional cubic spline functions of the fiber length, fiber velocity and activation.

$$K^m = \frac{\partial F^m(a, l^m, v^m)}{\partial \bar{l}^m} \tag{2}$$

The tendon stiffness K^t is obtained from the derivative of the tendon force-strain curve (Zajac 1989) in the instantaneous tendon strain value. Then, the stiffness of the MTU is derived according to the Hill-type muscle model, in which the muscle and the tendon are in series.

$$K^{MTU} = \frac{K^m \cdot K^t}{K^m + K^t} \tag{3}$$

- **D: MTU joint dynamics block.** The joint moment of the DOF of ankle plantar-dorsi flexion is computed as the sum of the product of each MTU force, F^{MTU}, and their associated moment arm, r. The stiffness of each MTU is projected at the joint level by the following equation:

$$K^j = \sum_{i=1}^{\#MTU} K_i^{MTU} \cdot r_i^2 + \frac{\partial r_i}{\partial \theta^A} \cdot F_i^{MTU} \tag{4}$$

where K^A is the ankle joint stiffness, K_i^{MTU} the stiffness of the i^{th} MTU, r_i the moment arm of the i^{th} MTU, θ^A the ankle angle and F_i^{MTU} the force in the i^{th} MTU .
- **E: Calibration block.** Before the EMG-driven musculoskeletal model can be run in open-loop to predict muscle forces and joint torques, it needs to be calibrated. In this step, an optimization routine adjusts certain subject-specific model parameters in order to minimize the error between the estimated and experimental torques (provided by the Achilles). The adjusted parameters are the tendon slack length, the optimal fiber lengths of the modeled muscles and a strength coefficient for each MTU. Additionally, three more coefficients that describe the non-linear muscle activation dynamics are optimized. A detailed description of the model parameters is provided in Pizzolato et al. 2015.

C. Dynamic Model for Short-Range Stiffness

In this study we considered that the main mechanism of the muscles in response to perturbations results from short-range stiffness. In order to account for SRS we extended the Hill-type muscle model by including a component parallel to the muscle, as it was suggested by de Groote, Allen, and Ting 2017 (Fig. 2). The behavior of the force produced by short-range stiffness was modelled as a function of the stretch of the muscle fiber. SRS was computed only during lengthening. The force produced by the muscle due to short-range stiffness will be referred to in the rest of this study as ”short-range stiffness force” (SRS force). The SRS force is proportional to the fiber stretch at each instant of time δ. However, from a certain critical stretch, δ_c, SRS is proportional to that constant critical stretch. The calculation

[1]https://simtk-confluence.stanford.edu/display/OpenSim/Gait+2392+and+2354+Models

[2]https://simtk.org/projects/ceinms

of SRS force is computed by the same approach as suggested by de Groote, Allen, and Ting 2017.

$$F_m^{SRS}(a,\bar{l}^m,\Delta\bar{l}^m)=\begin{cases}0 & ,if \Delta\bar{l}^m<0\\ \gamma F_m^0 a f_{act}(\bar{l}^m)\Delta\bar{l}^m & ,if 0<\Delta\bar{l}^m<\delta_c\\ \gamma F_m^0 a f_{act}(\bar{l}^m)\delta_c & ,if \Delta\bar{l}^m>\delta_c\end{cases} \tag{5}$$

where $\gamma = 280$ is the short-range stiffness constant, F_m^0 is the maximal isometric muscle force, $f_{act}(\bar{l}^m))$ is the muscle force-length relation, $\bar{l}^m$ is the fiber length normalized by optimal fiber length , $\Delta\bar{l}^m$ is the normalized fiber stretch, a is the activation of the muscle fiber, and $\delta = 5.7 \cdot 10^{-3}$ is the normalized critical stretch. The normalized fiber stretch is computed in relation to the stretch of the fiber at the instant of the perturbation (Eq. 6).

$$\Delta\bar{l}^m = \frac{l^m - l_p^m}{l_0^m} \tag{6}$$

where l_p^m is the fiber length at the instant of the perturbation, l^m is the muscle fiber length and l_0^m, is the optimal fiber length. As discussed previously, SRS does not only depend on the fiber stretch. Only after 50ms of the perturbation time, the first changes in activation due to spinal cord signals occur and the active mechanism of the fibers becomes dominant over SRS (de Groote, Allen, and Ting 2017). Therefore, the contribution of SRS as described in Eq. 5 was only computed during the time window of 50 ms after a perturbation.

Although a model for the force produced by SRS was proposed by de Groote, Allen, and Ting 2017, no derivation of stiffness from the muscle force was calculated. To compute short-range stiffness we used an adaptation of the approach suggested by Cui et al. 2008, in which the stiffness of the muscle is given by the following equation:

$$K_m^{SRS} = \beta(A)\frac{\partial F_m^{SRS}}{\partial \bar{l}^m} \tag{7}$$

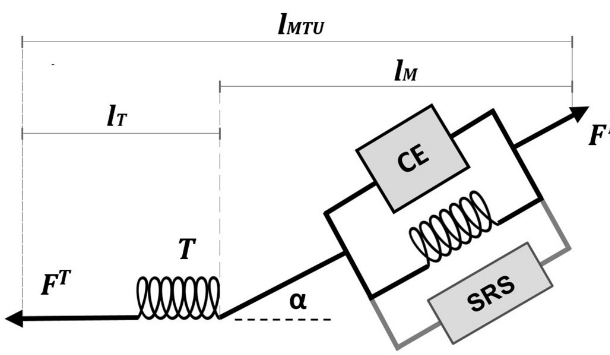

Fig. 2: Modified Hill-type muscle model, with short-range stiffness. The MT-actuator comprises of a tendon T, in series with a muscle.The muscle consists of a contractile element, CE, parallel to a passive element. In the short-range regime, another parallel element is added within the muscle model to account for the contribution of short-range stiffness. The pennation angle α is the angle between the orientation of the muscle fibers and the tendon.

where F_m^{SRS} is the muscle SRS force, $\bar{l}^m$ is the normalized fiber length and $\beta(A)$ is a multiplicative factor, that will be explained shortly. The same approach was used by Cui et al. 2008 to calculate muscle stiffness from muscle force. However, in this study instead of a constant value, the derivative of the muscle force was multiplied by a parameter β, that varied with the maximal amplitude of the muscle fibers throughout the entire movement, A. The parameter β was designed to have an exponential decay with the amplitude of the muscle fibers (Eq. 8, Appendix B: Fig. 11).

$$\beta(A) = Ge^{-B\cdot A} \tag{8}$$

where G represents the gain of the function $\beta(A)$, B is a shape factor to model how fast β decays with the amplitude and A is the maximal amplitude of each muscle fiber throughout the entire movement. In this study, B was considered constant (B = 200). In contrast, G was optimized for each subject and each trial between a value ranging from $[0 \quad 40]$ (Section II.D). This parameter aimes to mimic the rate of formation and deformation of cross-bridges. Hence, in large amplitudes of movement there is a high rate of formation and deformation of cross-bridges, reducing the contribution of SRS. Contrarily, during small amplitudes of movements, the rate of formation and deformation of cross bridges is small, so more contribution of SRS is expected (Joyce, P. Rack, and Westbury 1969; P. M. Rack and Westbury 1974).

Subject specific splines for SRS force (Eq. 5) and SRS (Eq. 7) were calculated for all the possible combinations of fiber activation, fiber lengths and fiber stretch (Appendix A Fig. 9), in order to avoid discontinuities while computing the force derivative. To adapt the EMG-driven musculoskeletal modeling framework described in Section II.B to include the computation of SRS, a few changes in the described blocks were made. To the block C, the computation of SRS force and SRS (Eq. 5 and Eq.7) was added. This computation was only triggered during the period of the initial mechanical response after each perturbation. Consequently, the force in the muscle during the short-range regime is the summation of the force in the muscle from the Hill-type muscle model (F^m) plus the force from SRS (F^{SRS}).

Since one more component was added in parallel with the muscle in the Hill-type muscle model, the calculation of the MTU stiffness is given by:

$$K^{MTU} = \frac{(K^m + K^{SRS})\cdot K^t}{K^m + K^{SRS} + K^t} \tag{9}$$

In block D of the EMG-driven model the computation of joint dynamics is made by using the muscle force and MTU stiffness as referred to above.

The force in the muscle from the Hill-type muscle model (F^m) is given by:

$$F^m = a(t)f(\bar{l}^m)f(\bar{v}^m) + f_p(\bar{l}^m) \tag{10}$$

In order to verify the influence of fiber velocity in the SRS response, we run the model with and without the contribu-

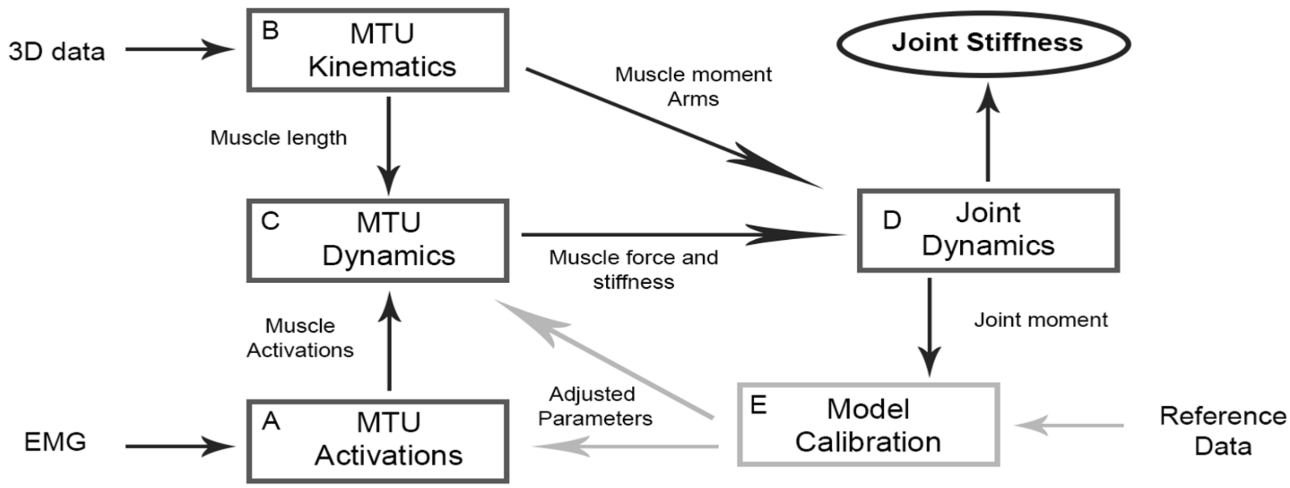

Fig. 3: Schematic diagram of the EMG-driven musculoskeletal modeling pipeline used in this study. It consists of five blocks: model calibration, MTU activation, MTU kinematics, MTU dynamics, and joint dynamics. Firstly, the model calibration block uses EMG-signals, three-dimensional (3D) joint angles and experimental ankle torques from several calibration trials to find the optimal set of model parameters that enable the computation of the ankle torque that best fits the experimental torque. The MTU activation block maps the EMG activity recorded from five muscles to activations for seven MTUs. The MTU kinematics block derives MTU lengths and moment arms from experimental 3D ankle angles. MTU force and stiffness are computed as a function of MTU activation and MTU kinematics in the MTU dynamics block. Lastly, the joint torque and stiffness are obtained by projecting the resulting MTU forces and stiffness on the ankle plantar-dorsi flexion degree of freedom in the joint dynamics block. Adapted from (Sartori, Maculan, et al. 2015).

tion of the force-velocity curve ($f(\bar{v}^m)$) to the viscoelastic response of the muscle (Eq. 10).

D. Dynamic Modulation of SRS

As explained earlier in this section, the parameter β that accounted for the different range of motion of each fiber was optimized for each subject and for each task. This optimization was only applied to the gain parameter (G) in the expression of β (Eq. 8). The optimization algorithm consists of several steps.

1) Find a value of G within $[Gmin \quad Gmax]$. Only integer values where computed.
2) Compute the value of β by Eq. 8.
3) Compute short-range stiffness for each muscle by (Eq. 7).
4) Compute the global MTU stiffness, accounting for the SRS contribution (Eq. 9).
5) Project the stiffness of each MTU into the joint level to obtain the dynamic joint stiffness (Eq. 4).
6) Compute the value of the cost function. The cost function used in this optimization was based on the same approach used to calibrate the EMG-driven musculoskeletal modeling framework during the calibration step (Section II B). However, in this case, the difference between the estimated joint stiffness and the stiffness obtained during system identification was minimized (Eq. 11).

$$f(K) = \frac{1}{N_r} \sum_{r=1}^{\#rows} \frac{(K^j - K^{ref})^2}{VAR(K^{ref})} \tag{11}$$

where K^j, is the estimated stiffness, K^{ref} is the stiffness obtained from system identification, VAR(K^{ref}) is the variance of the stiffness from system identification and N_r is the number of samples of the signals.
7) The new value of G was accepted if the value of the objective function was smaller than with the previous value of G.
8) The algorithm runs until all the solution space had been evaluated, i.e. until G had taken all integer values between $Gmin$ and $Gmax$.

When the algorithm ended, an optimal value of G was obtained. This value minimized the difference between the model estimated stiffness and the stiffness from system identification. The limit values of the parameter G were chosen in order to obtain values of short-range stiffness not lager than 10 times higher the stiffness computed from the standard Hill-type muscle model. As a result, the values considered for $Gmin$ and $Gmax$ were 0 and 40, respectively.

E. Fibre stretch detection algorithm

Since SRS only contributes to the response of the muscle in the presence of a perturbation, a method to trigger the computation of SRS was required. In the profile of the muscle acceleration for each muscle fiber a clear and repetitive patterns were observed when a perturbation was applied. To detect these changes in muscle fiber acceleration, two symmetrical wavelets were designed, representing both perturbation types, in the direction of dorsi flexion and in the direction of plantarflexion. Then, the acceleration profile for each muscle was scanned and the root mean squared error (RMSE) between the acceleration and each wavelet was calculated, resulting in a structure with multiple values of RMSE at each scanning point. The values of RMSE was manipulated mathematically to have clear distinguished peaks on the RMSE, as follows: 1) remove the offset of the RMSE; 2) Invert the values RMSE; 3) raise to the third power. In this way, the lowest values of RMSE between the acceleration profile and the scanned signals became the highest points. A threshold was applied to select the highest peaks for each muscle. Finally, some acceptance conditions needed to be met to consider these highest peaks perturbations. Those conditions were:

1) The perturbations within the same muscle were at least 50ms apart.
2) The same perturbation between different muscles were at least within the same 10ms window.
3) Each perturbation needed to be detected in at least three different muscles.

These conditions allowed to guarantee that a single perturbation was detected within the time span of the short-range regime, so the effect of SRS was not multiplied, which would not provide a situation physiologically possible. Please note that this methodology could be implemented during real-time modeling, since the only variable required was acceleration that was obtained by the derivative of the fiber velocity, which was provided by the model.

F. Data Analysis

The EMG-driven model together with the SRS model was validated at the stiffness level by comparing with the results obtained by system identification. In system identification techniques, only one stiffness trajectory for the plantar-dorsi flexion cycle was obtained. Therefore, during the optimization algorithm (Section II D.) and to compare the dynamic stiffness obtained by the model with the stiffness from system identification stiffness, the different cycles of each trial were extracted and subsequently interpolated and time-normalized using cubic splines. Each cycle was defined as a complete period of the torque profile (from minimum to minimum). SRS only induced a positive summation effect on the muscle force and stiffness so the stiffness values estimated with the model including SRS were not normally distributed. Consequently, statistical analysis on this data might result in some misinterpretation, especially in the stiffness plots where standard deviation (STD) is shown as the region around the mean curve due to the summation and subtraction of the value of STD at each point. Hence, the negative values of stiffness do not reflect the data. Results were compared both in shape and magnitude by the coefficient of determination (R2, square of the Pearson product moment correlation coefficient) and the RMSE, respectively.

III. RESULTS

Before implementing SRS, the behaviour of the SRS variables during the perturbations timing was evaluated. In Fig. 4 the torque, angle and activation trajectories for one profile cycle are depicted.

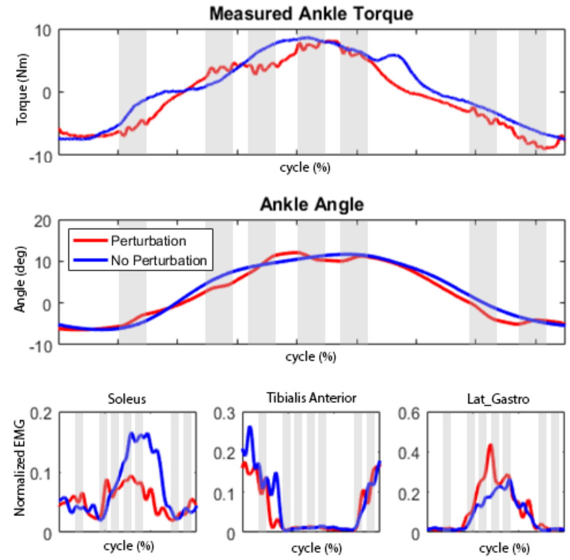

Fig. 4: Representative cycle for the measured Achilles torque (top), ankle angle (middle) and normalized EMG (bottom). The red and blue lines represent the profile with and without applied perturbations, respectively. The shaded grey areas represent the period of 50ms after the instant of each perturbation.

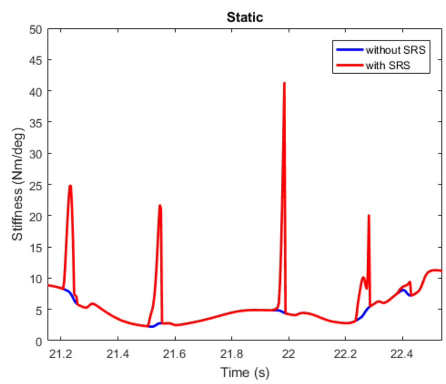

(a)

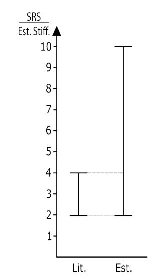

(b)

Fig. 5: 5a: Estimated joint stiffness for a single representative cycle. The red line represents the estimated stiffness by including SRS in the EMG-driven model. The blue line represents the estimated joint stiffness without including SRS in the model. 5b: Comparison of the ratio between SRS and dynamic stiffness from the literature values and the model estimated values.

Although it was hard to quantify changes in the profile of the normalized EMG signal due to its noise, no clear changes on the EMG pattern at the time of the perturbation were detected. Contrarily, a clear change in the torque measured by the Achilles and a smaller but still noticeable change in joint angle were detected (Fig. 4). These evidences support our hypothesis that changes in joint torque during the perturbation period must result from intrinsic muscle properties.

TABLE I: Comparison of Stiffness Estimations via EMG-driven modeling and system identification, with and without the contribution of SRS. Values of RMSE and R^2 for each subject and average between subjects.

	Dynamic 0.6Hz				Dynamic 0.3Hz				Static			
	RMSE		R^2		RMSE		R^2		RMSE		R^2	
	No SRS	SRS	No SRS	SRS	No SRS	SRS	No SRS	SRS	No SRS	SRS	No SRS	SRS
Sub1	7.18	7.18	0.75	0.75	12.96	12.93	0.00	0.00	9.62	7.87	0.64	0.15
Sub2	8.09	8.09	0.00	0.00	15.73	15.71	0.05	0.04	16.87	16.16	0.01	0.07
Sub3	8.63	8.44	0.55	0.55	13.50	13.87	0.33	0.31	10.28	8.75	0.01	0.04
Sub5	6.35	6.31	0.17	0.18	16.01	15.89	0.01	0.01	12.09	11.49	0.44	0.37
Sub6	8.73	8.67	0.08	0.07	10.86	10.57	0.00	0.00	16.24	15.42	0.46	0.30
Total	4.33	4.34	0.35	0.35	12.55	12.41	0.07	0.07	12.52	11.40	0.21	0.15

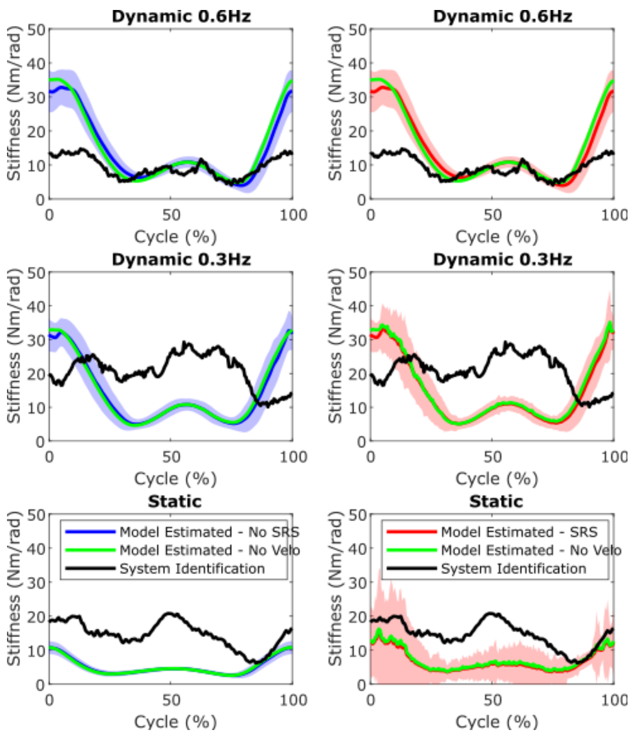

Fig. 6: Comparison of the stiffness estimations of the proposed model against system identification techniques for the dynamic task at 0.6Hz (top), dynamic task at 0.3Hz (middle) and static task (bottom). The left column contains the values of estimated stiffness without including SRS (blue) and the right column contains the values of estimated stiffness by including SRS (red) in the EMG-driven model. The green lines represent the estimated stiffness without the contribution of the force-velocity curve to the muscle force response. The bold line represents the average stiffness across cycles obtained, in each respective case, by the EMG-driven model, and the shaded area corresponds to the standard deviation. The thick black line represents the stiffness estimation via system identification.

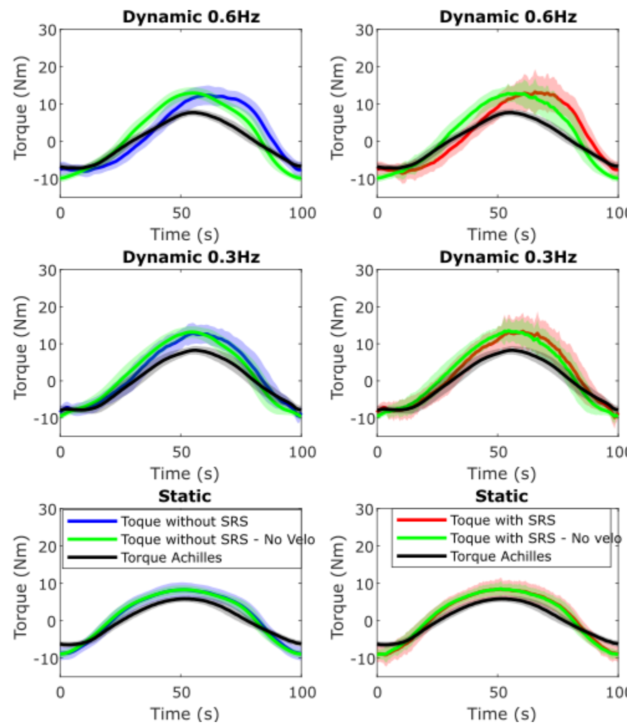

Fig. 7: Comparison of the torque estimations of the proposed model against Achilles measured torques for the dynamic task at 0.6Hz (top), dynamic task at 0.3Hz (middle) and static task (bottom). The left column contains the values of estimated stiffness without including SRS (blue) and the right column contains the values of estimated stiffness by including SRS (red) in the EMG-driven model. The green lines represent the estimated stiffness without the contribution of the force-velocity curve to the muscle force response. The black curve represents the average torque estimation by the Achilles device. The bold line represents the average stiffness across cycles obtained, in each respective case, and the shaded area corresponds to the standard deviation.

A. SRS model

First an example of the behavior of the modelled joint stiffness with the addition of SRS is provided. In Fig. 5, the profile of joint stiffness computed by the EMG-driven model without SRS (blue) and with the contribution of SRS (red) is shown for only one representative cycle. At the time of each perturbation, a spike in the joint stiffness profile was observed, which reflected the projection of the fast increase in short-range stiffness for each muscle (Eq. 7) at the joint level.

Estimated joint stiffness for all subjects and trials can be found in Appendix D Fig. 14. Subject 4 was excluded from the analysis due to abnormalities in EMG signals, as reported by Cop et al. 2019. The model estimated joint stiffness was averaged across all the cycles recorded for each task and

TABLE II: Mean values of β and maximum fibre length amplitude. The values are represented as a mean $\pm$ standard deviation. The values are averaged across all repetitions and all subjects for the same task for each muscle fiber.

Mean Values of β			
	Dynamic 0.6Hz	Dynamic 0.3Hz	Static
LatGas	0.15 $\pm$ 0.24	0.38 $\pm$ 0.32	15.77 $\pm$ 5.54
MedGas	0.22 $\pm$ 0.30	0.54 $\pm$ 0.41	18.72 $\pm$ 3.20
PerBrev	7.23 $\pm$ 8.19	14.25 $\pm$ 8.45	28.92 $\pm$ 4.57
PerLong	4.16 $\pm$ 4.74	8.22 $\pm$ 5.01	23.57 $\pm$ 6.80
PerTert	0.64 $\pm$ 0.71	1.60 $\pm$ 0.94	23.09 $\pm$ 1.10
Soleus	0.31 $\pm$ 0.40	0.75 $\pm$ 0.56	20.79 $\pm$ 2.98
TibAnt	0.10 $\pm$ 0.12	0.29 $\pm$ 0.20	15.38 $\pm$ 1.59

Maximum fiber length amplitude (cm)			
	Dynamic 0.6Hz	Dynamic 0.3Hz	Static
LatGas	2.04 $\pm$ 0.30	1.92 $\pm$ 0.26	0.41 $\pm$ 0.15
MedGas	1.72 $\pm$ 0.21	1.66 $\pm$ 0.17	0.32 $\pm$ 0.07
PerBrev	0.29 $\pm$ 0.04	0.28 $\pm$ 0.05	0.14 $\pm$ 0.06
PerLong	0.51 $\pm$ 0.05	0.51 $\pm$ 0.09	0.24 $\pm$ 0.13
PerTert	1.23 $\pm$ 0.11	1.18 $\pm$ 0.07	0.23 $\pm$ 0.02
Soleus	1.54 $\pm$ 0.21	1.51 $\pm$ 0.19	0.27 $\pm$ 0.06
TibAnt	2.02 $\pm$ 0.23	1.92 $\pm$ 0.17	0.4 $\pm$ 0.04

then compared to the one obtained via system identification (SI). In Fig. 6, the stiffness profile of the estimated stiffness against the stiffness from system identification (black curves) for one representative subject is presented. In the left column the stiffness estimated without including SRS is shown and in the right column the estimated stiffness by including SRS in the EMG-driven model is depicted, as suggested in this study. Additionally, the values of joint stiffness obtained without the contribution of the force-velocity curve to the muscle response are also plotted (green curves). From the figure, it is clear that the joint stiffness profile during fast dynamic tasks (0.6 Hz) was not altered in comparison with the model without SRS. However, for slow dynamic tasks (0.3 Hz), and especially static tasks, the mean trajectory of the joint stiffness estimated by the model with SRS was closer to the values of system identification than the joint stiffness computed without SRS. The same results were obtained by looking at the values of RMSE and R^2 in Table I. The same results were obtained for all subjects, showing no changes in the fast dynamic task, smaller changes in the slow dynamic tasks and considerable changes in the static tasks. Although the values of RMSE and R^2 were better for some subjects, all subjects showed better results by including SRS in the model. Further, no large differences of the joint stiffness profile were observed when the contribution of the force-velocity curve was removed from the muscle response.

The maximum value of joint stiffness throughout different percentages of the plantar-dorsi flexion cycle can be seen in the histogram in Fig. 8. In the histogram the mean of the maximum values of stiffness for each condition within a certain percentage of the cycle are shown against the mean maximum stiffness for the same percentage of the cycle without the contribution of SRS. We can observe that joint stiffness due to SRS is on average 2 to 10 times higher than the joint stiffness without the presence of SRS. SRS is not constant in the entire cycle, being more predominant in the peaks of plantarflexion and dorsiflexion. At the muscle level the values of short-range stiffness varied also between 2 to 10 times higher than the stiffness from the standard Hill-type muscle model. The values of maximum stiffness at the muscle level are shown in Table V on the Appendix A.

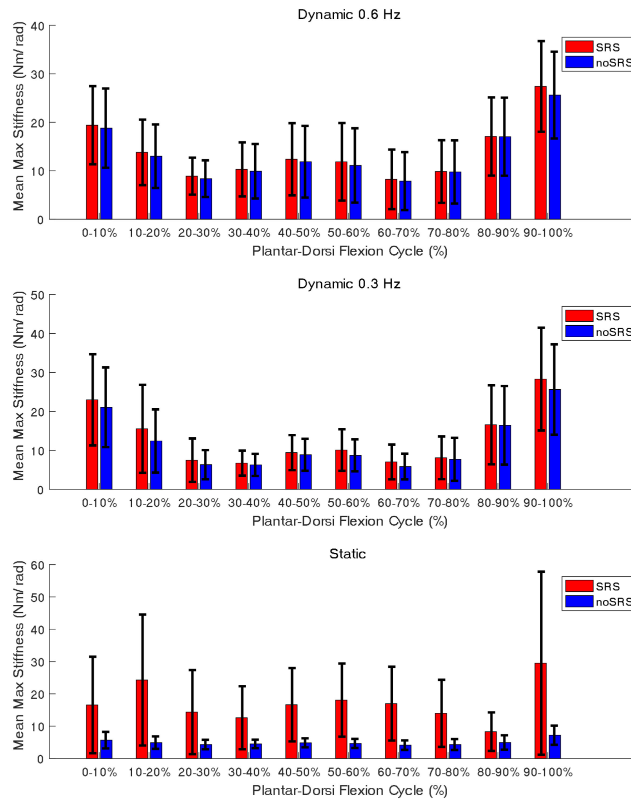

Fig. 8: Maximum values of joint stiffness for different percentages of the plantar-dorsi flexion cycle, averaged across all subjects. Plots for the dynamic task at 0.6Hz (top), dynamic task at 0.3Hz (middle) and static task (bottom). The red bars represent the mean of the maximum values of joint stiffness with the contribution of SRS within the corresponding percentage. The blue bars represent the mean of the maximum values of joint stiffness without the contribution of SRS for a certain percentage of the cycle. The black error bars represent the standard deviation of these maximum values.

B. Torque Response

After looking into the stiffness profile, the torque response was also analyzed for the same presented conditions. The model estimated torque was compared to the experimental torque obtained by the Achilles device (Fig. 7 black curve). The influence of SRS in the torque profile is considerably lower than in the stiffness profile. Contrarily to what was

TABLE III: Fibre stretch detection rate. Percentage of successes (Succ), false positives (FP) and false negatives (FN) for each subject and average over all subjects (Total).

	Dynamic 0.6 Hz (%)			Dynamic 0.3 Hz (%)			Static (%)		
	Succ	FP	FN	Succ	FP	FN	Succ	FP	FN
Sub1	89	1	10	99	0	1	98	1	1
Sub2	81	4	15	94	0	6	96	4	0
Sub3	90	0	10	98	0	2	99	1	0
Sub5	84	6	10	93	0	7	88	12	0
Sub6	81	0	19	96	0	4	99	0	1
Total	85±4	2±3	13±4	96±3	0±0	4±3	96±5	3±5	0±0

TABLE IV: Fibre stretch detection rate. Percentage of perturbations detected with 0ms error (exact), within a 8ms window ($<$ 8ms) and within a 27ms window ($<$ 27ms)

	Dynamic 0.6 Hz (%)			Dynamic 0.3 Hz (%)			Static (%)		
	Exact	<8ms	<27ms	Exact	<8ms	<27ms	Exact	<8ms	<27ms
Sub1	31	57	1	36	62	1	36	62	0
Sub2	13	35	34	12	38	44	19	47	30
Sub3	26	60	3	30	65	3	33	66	0
Sub5	0	30	54	1	39	53	0	21	68
Sub6	9	71	1	2	93	1	0	86	13
Total	16 ± 13	50 ± 17	19 ± 24	16 ± 16	59 ± 23	20 ± 26	17 ± 17	56 ± 24	23 ± 28

obtained for the stiffness profile, the torque profiles obtained without the contribution of the force-velocity curve to the muscle response in some cases greatly differ from the complete model estimations.

C. Optimization Algorithm for Short-range Stiffness Calculation

The optimization algorithm was applied to find the best value of gain, G, for the parameter β, which was multiplied with the derivative of the SRS force in order to obtain the value of short-range stiffness for each muscle fiber (Eq. 8). An optimal value of G was found for all the trials and all the subjects, between a minimum value of 0 and a maximum value of 40. The mean values of the parameter G over all subjects and all repetitions were: 14 $\pm$ 13 for the dynamic 0.6 Hz task, 28 $\pm$ 15 for the dynamic 0.3 Hz and 40 $\pm$ 0 for the static task. It was clear that the values G are lower for the dynamic task than for the static task, and lower in the fast dynamic task (0.6 Hz) than in the slow dynamic task (0.3 Hz). A low value of G represented a low contribution of SRS. The maximum variation of fiber length throughout the all cycle of plantar-dorsi flexion together with the correspondent values of the parameter β for each muscle fiber are represented in Table II. We realized that fibers with lower variations in length, such as the Peroneus Brevis and Peroneus Longus, had higher values of the parameter β compared to fibers with large amplitude of movement. The optimization algorithm took about 3% of the total time that the EMG-driven modeling framework took to compute joint stiffness.

D. Fibre stretch detection

The algorithm to trigger SRS was designed with the goal to detect the perturbations applied by the Achilles Rehabilitation device. The detection rates of the designed algorithm were compared with the actual instants of the perturbations obtained from an output file from the Achilles device. The algorithm detected always above 80% of the perturbations in all tested conditions. In fast dynamic conditions the algorithm performed worse than in slow dynamic conditions and in static dynamic conditions. On the latter two tasks the algorithm always detected above 90% of the perturbations applied. From Table III we verify that the average number of false positives was lower than the number of false negatives, meaning that the algorithm missed more often the detection of a perturbation than considered it a success when there was no perturbation. A perturbation was considered detected (or a success) if it was found within an interval of 27ms of the actual timing of the perturbation. Then, three different categories were analyzed for the rate of successes. A perturbation was detected on the exact time of the real perturbation (Exact), a perturbation was detected within an interval of 8ms of the real perturbation or the perturbation was detected in an interval of 27ms of the real perturbation. In Table IV, these rates of detection are reported. It is important to note, that the number of detection of each category are exclusive from the previous ones, i.e., the 27ms interval does not include perturbations detected within a 8ms window or at the exact time, and in the 8ms interval no perturbations detected at the exact time are included. Therefore, most of the perturbations were detected within the 8ms window.

IV. Discussion

This project developed an innovative methodology to implement short-range stiffness in an EMG-driven musculoskeletal modeling framework to improve the estimation of joint stiffness during different types of movements. Firstly, the Hill-type muscle model implemented in the modeling framework was adapted to account for the force produced in the muscles due to SRS. Secondly, an optimization routine to adapt the computed muscle SRS to the characteristics of the performed movement was developed. Third, and lastly, an automatic detection algorithm was included in the framework to trigger the computation of SRS during the whole movement. For the first time a model of SRS was developed and tested in different types of dynamic and static tasks and showed improvements on the estimated joint stiffness. Additionally, the proposed method does not require any additional information to transition between the compliant and the short-range regime of the muscle, mimicking the physiological behaviour of the muscles.

The perturbations applied to the ankle joint induced rotations of 0.03 rad. These rotations were about 2.5% of the physiological range of motion of the joint, therefore we assumed that the perturbations occurred within the short-range regime (P. M. Rack and Westbury 1974). During the 50ms after the instant of the perturbation, we verified a rapid change in joint torque followed by a delayed change in joint angle and no significant changes in muscle activity. Based on this evidence, we postulated that observed changes in torque during this short period of time cannot result from active muscle response, but they must result from intrinsic muscle properties. These observations agreed with the short-range conditions reported by de Groote, Allen, and Ting 2017.

The estimated joint stiffness was compared with the values of stiffness obtained from system identification. System identification techniques provided a value of stiffness for one cycle of plantar-dorsi flexion by averaging across a large amount of cycles. Contrarily to what is estimated via musculoskeletal modeling, with system identification techniques it is not possible to obtain an instantaneous value of joint stiffness (Lee, Rouse, and Krebs 2016, Weiss, Hunter, and Kearney 1988). The two stiffness values result from distinguished measurements which can not always reflect the same quantity. Therefore, we should be conservative when comparing both stiffness values.

The model with the inclusion of SRS estimated joint stiffness more accurately than the model without SRS, especially during static tasks (Fig. 6). In fast dynamic tasks there was no difference in the estimation of joint stiffness between the model with or without SRS. This result was expected since in dynamic tasks the rate of formation and deformation of cross-bridges is very high which results in a lower contribution of SRS for the resulted muscle force (Joyce, P. Rack, and Westbury 1969; Ettema and Huijing 1994). On the other hand, for static tasks the rate of formation and deformation of cross-bridges is lower, resulting in a higher number of cross-bridges attached at the time of the perturbation and, consequently, inducing a higher contribution of SRS to the total muscle force (Joyce, P. Rack, and Westbury 1969). However, while the mean over multiple cycles was closer from the stiffness obtained by system identification, a large standard deviation was obtained when including SRS in the framework. This large standard deviation can be due to multiple reasons. In static conditions, the initial position of the foot could be slightly different between repetitions which originated in differences in fiber stretch when averaging across all cycles of all repetition. Consequently, the values obtained for fiber stretch were also very noisy. Moreover, SRS was only computed during lengthening and perturbations were randomly applied during the whole cycle, so depending on the movement of each muscle fiber at the time of perturbation, the SRS response could be different. Since the model of SRS suggested in this study involved a large amount of variables that changed during the movement cycle and differently with each muscle, a prediction could be that the number of cycles used for each condition were not greater enough to verify more consistency in the results during the entire movement cycle. Another important factor could be the value of the SRS constant, which was chosen between certain limits based on previous studies performed in different types of task. So a suggestion to improve the estimation of SRS will be to better tune this parameter.

Since the comparison at the stiffness level could be controversial, we analyzed the estimated torque profile and compared it with the experimental torque obtained with the Achilles device. The calibration of the EMG-musculoskeletal model performed prior to this study (Cop et al. 2019) was also performed at the torque level. During calibration, subject-specific parameters were optimized in order to minimize the error between the experimental torque and the estimated torque. The calibration was performed by modelling each MTU with a standard Hill-type muscle model without including the suggested model of SRS. Hence, as SRS is the mechanism used by the muscle to respond to a perturbation but it was not accounted during the model calibration, an overestimation of the model estimated torque at the time of the perturbations was observed (Appendix D, Fig 15). These observations support the fact that the calibration of the model should be performed with the inclusion of the suggested model of SRS in the muscle model. In this way, also the parameters that define the SRS model can be optimized together with the subject-specific parameters to obtain a better physiological representation of the muscle response.

As discussed previously, the type of movement influenced the displacement of each muscle fiber, which could be different between muscle fibers. So, each muscle fiber could have a different short-range stiffness response (P. M. Rack and Westbury 1974; Hufschmidt and Schwaller 1987). In this study, we verified that the Peroneus Brevis and Peroneus Longus do not have large changes in fiber amplitude during the plantar-dorsi flexion cycle in comparison with other muscles in the model (Table II). Therefore, the contribution of these two muscles to SRS was expected to be larger than muscles that suffered larger amplitude of movement. This characteristic was mimicked by the parameter β. This parameter was multiplied by the derivative of the muscle SRS force with respect to the normalized fiber length to obtain the value of SRS for each muscle fiber. This parameter could vary from 0 to 40, representing no contribution of SRS to large contribution of SRS, respectively. For dynamic tasks this parameter was around 5 for the Peroneus Brevis and Peroneus Longus and around 0 for all the other muscles. Differently, for static tasks values of β were around 25 for the Peroneus Brevis and Peroneus Longus and around 18 for the rest of the muscles.

For slow dynamic tasks a large standard deviation was obtained for the contribution of SRS, specifically in the values of G. As can be seen in Fig. 14 the profile of the joint stiffness for this condition varied substantially between subjects and the shape of the estimated stiffness not always corresponds to the shape of the stiffness from system identification. Therefore, this can result from calibration issues of the model as reported in the previous study (Cop et al. 2019), which go out of the scope of the present study. Moreover, the contribution of SRS in slow dynamic tasks is still unclear. On the one hand, muscle fibers do suffer changes in length, although at a slow rate of formation and deformation of cross-bridges, so the number of cross-bridges formed at each instant of time should be lower than in static condition. On the other hand, slow movements implicitly suggest that cross-bridges are attached during a longer period of time than in faster movements, so a perturbation could still induce a certain amount of cross-bridge deformation reflecting an increase in SRS response. The same relation between amplitude of the movement and short-range stiffness was also reported by P. M. Rack and Westbury 1974.

In respect to the influence of velocity to the SRS response, literature had reported that the magnitude of SRS does not vary with the velocity of the muscle fiber, although the duration of the short-range regime varies considerably with the fiber velocity (P. M. Rack and Westbury 1974). In our approach no clear changes with or without the contribution of the force-velocity curve were observed. However, the maximum contraction velocity, used to normalize the fiber velocity, was considered constant across subjects and across muscle fibers. Consequently, a single type of muscle fibers are modelled. A deeper research will be required to understand the influence of modelling fibers with different contraction velocities, fast and slow fibers, to the response to perturbations.

The limit value of the parameters β was chosen in order to obtain values of short-range stiffness not lager than 10 times higher than the stiffness computed from the standard Hill-type muscle model (Sartori, Maculan, et al. 2015). The maximum values of SRS were between 600 to 10000 Nm/rad depending on the muscle fiber. These results are hardly compared with the ones in literature, since no values of muscle specific short-range stiffness have been published. At the joint level we obtained values of joint stiffness during the short-range regime about 2 to 10 times higher than during the complaint regime, i.e. a maximum joint short range stiffness of about 100 Nm/rad. Hun et al. reported values of elbow SRS of about 50 to 100 Nm/rad for joint torques from -10 to 10 Nm/rad (Hu, Murray, and Perreault 2011). A previous study reported values of ankle stiffness between 50 to 150 Nm/rad for the same values of torque (Hunter and Kearney 1982). Although the values obtained in the present study are in the same interval as the values reported in previous studies, we cannot neglect the fact that the previous studies were performed in tasks that guarantee the muscles were always within the short-range regime. So, the force response produced by the muscle can be considerably different. The suggested optimization algorithm accounts for the total amplitude change of the fiber length during the entire cycle to compute β and further on SRS. So, in order to implement this methodology in real-time is required to know in advance which is the average change in length that each muscle fiber suffers during the performed movement. A future work could rely on adjusting this optimization in order to adjust the SRS based on a parameter obtained during real-time modeling.

All current SRS models in literature require a clear starting point to trigger SRS, i.e., muscles fibers were assumed to have no change in length and/or activation before a sudden single perturbation or displacement was applied (de Groote, Allen, and Ting 2017; Hu, Murray, and Perreault 2011; de Vlugt et al. 2011). When modeling SRS in dynamic tasks an evident limitation related with the activation of this response mechanism arises. In this study, a method that analyzed the acceleration profile of all muscle fibers and detected features to trigger the SRS mechanisms was developed. This detection algorithm showed good results, with detection rates always above 85% for all performed tasks. The lower detection rates where obtained during the fast dynamic tasks, however in these tasks a lower contribution of SRS is expected. To the current knowledge of the author, no algorithm to detect perturbation using muscle kinematics has been developed. Besides the good detection rates obtained, the algorithm is very conservative on the acceptance conditions and it was only tested for the same type of perturbations. In order to apply this method to larger scale movements, improvement of the algorithm will be required. A suggestion would be to analyze the effect of different types of perturbations in the muscle kinematics and develop more a more accurate detection algorithm. These methods could use wavelet transform together with machine learning in order to account for a variety of possible external perturbations.

Besides short-range stiffness, other history-dependent muscle mechanisms are not included in the standard Hill-type muscle model, such as stretch-induced force enhancement and shortening-induced force depression. Moreover, SRS can also be influenced by history-dependent characteristics, having its contribution diminished by multiple cycles of the same task (Campbell and M Lakie 1998). Including this characteristic into the musculoskeletal model can help improve the estimation of stiffness and also modulate the SRS contribution.

V. CONCLUSION

This study implemented SRS in a EMG-driven musculoskeletal modeling framework, with the goal to improve the estimation of joint stiffness in static conditions. Besides the implementation of the SRS model, the presented methodology also included a detection algorithm which triggers the computation of SRS without any additional information to the framework. Also, an optimization algorithm to account for the rate of formation and deformation of cross-bridges due to the amplitude of movement of the fibers was considered. Therefore, the entire methodology consists of a solid proof of concept for implementation of SRS in musculoskeletal models that can be applied to different types of movements indiscriminately.

Results showed that our model improved the estimation of joint stiffness for the static task without damaging the estimation of joint stiffness for dynamic tasks. High detection rates of the applied perturbations were also obtained. Although this project showed promising results for the implementation of SRS, the methodology was tested in a very confined movement. In order to extend the implementation of the model to a larger variety of movements, adjustments in the framework are required, such as accounting for multiple types of perturbations. Additionally, the inclusion of the SRS model during the calibration of the EMG-driven musculoskeletal model is recommended in order to obtain more physiological results.

Being able to accurately access instantaneous dynamic joint stiffness will have enormous implications in understanding human movement control, as well as the development of tailored neuro-rehabilitation therapies and biomimetic controlled prostheses and orthoses.

ACKNOWLEDGEMENTS

I would like to sincerely thank dr. Massimo Sartori for the kind support and close supervision of this Master assignment. I am also grateful to the PhD student MSc. Pablo Cop for his availability to help me during whole project. Finally, I want to show my appreciation to the examination committee: prof. Herman van der Kooij and prof. Jaap Buurke, for the interest in the project and the valuable feedback given.

REFERENCES

Campbell, KS and M Lakie (1998). "A cross-bridge mechanism can explain the thixotropic short-range elastic component of relaxed frog skeletal muscle". In: *The Journal of physiology* 510.3, pp. 941–962.

Cop, CP et al. (2019). "Model-based estimation of ankle joint stiffness during dynamic tasks: a validation-based approach." In: *41st EMB Conference (Submitted)*.

Cui, Lei et al. (2008). "Modeling short-range stiffness of feline lower hindlimb muscles". In: *Journal of biomechanics* 41.9, pp. 1945–1952.

Delp, Scott L et al. (2007). "OpenSim: open-source software to create and analyze dynamic simulations of movement". In: *IEEE transactions on biomedical engineering* 54.11, pp. 1940–1950.

de Groote, Friedl, Jessica L Allen, and Lena H Ting (2017). "Contribution of muscle short-range stiffness to initial changes in joint kinetics and kinematics during perturbations to standing balance: A simulation study". In: *Journal of biomechanics* 55, pp. 71–77.

de Groote, Friedl, Kyle P Blum, et al. (2018). "Interaction between muscle tone, short-range stiffness and increased sensory feedback gains explains key kinematic features of the pendulum test in spastic cerebral palsy: A simulation study". In: *PloS one* 13.10, e0205763.

de Vlugt, Erwin et al. (2011). "Short range stiffness elastic limit depends on joint velocity". In: *Journal of biomechanics* 44.11, pp. 2106–2112.

Eggleston, Jeffrey D, John R Harry, and Janet S Dufek (2018). "Lower extremity joint stiffness during walking distinguishes children with and without autism". In: *Human movement science* 62, pp. 25–33.

Ettema, GJC and PA Huijing (1994). "Skeletal muscle stiffness in static and dynamic contractions". In: *Journal of biomechanics* 27.11, pp. 1361–1368.

Galli, Manuela et al. (2018). "An examination of the relationship between dynamic knee joint stiffness and gait pattern of children with cerebral palsy". In: *Journal of bodywork and movement therapies* 22.3, pp. 747–751.

Getz, Elise Burmeister, Roger Cooke, and Steven L Lehman (1998). "Phase transition in force during ramp stretches of skeletal muscle". In: *Biophysical Journal* 75.6, pp. 2971–2983.

Hill, Archibald Vivian (1938). "The heat of shortening and the dynamic constants of muscle". In: *Proceedings of the Royal Society of London. Series B-Biological Sciences* 126.843, pp. 136–195.

Hu, Xiao, Wendy M Murray, and Eric J Perreault (2011). "Muscle short-range stiffness can be used to estimate the endpoint stiffness of the human arm". In: *Journal of neurophysiology* 105.4, pp. 1633–1641.

Hufschmidt, A and I Schwaller (1987). "Short-range elasticity and resting tension of relaxed human lower leg muscles." In: *The Journal of physiology* 391.1, pp. 451–465.

Hunter, IW and RE Kearney (1982). "Dynamics of human ankle stiffness: variation with mean ankle torque". In: *Journal of biomechanics* 15.10, pp. 747–752.

Joyce, GC, PMH Rack, and DR Westbury (1969). "The mechanical properties of cat soleus muscle during controlled lengthening and shortening movements". In: *The Journal of physiology* 204.2, pp. 461–474.

Latash, Mark L and Vladimir M Zatsiorsky (1993). "Joint stiffness: Myth or reality?" In: *Human movement science* 12.6, pp. 653–692.

Lee, Hyunglae, Elliott J Rouse, and Hermano Igo Krebs (2016). "Summary of human ankle mechanical impedance during walking". In: *IEEE journal of translational engineering in health and medicine* 4, pp. 1–7.

Loram, Ian D, Constantinos N Maganaris, and Martin Lakie (2007). "The passive, human calf muscles in relation to standing: the non-linear decrease from short range to long range stiffness". In: *The Journal of physiology* 584.2, pp. 661–675.

Martins, JAC et al. (1998). "A numerical model of passive and active behavior of skeletal muscles". In: *Computer methods in applied mechanics and engineering* 151.3-4, pp. 419–433.

McGowan, Craig P, RR Neptune, and W Herzog (2013). “A phenomenological muscle model to assess history dependent effects in human movement”. In: *Journal of biomechanics* 46.1, pp. 151–157.

Moya Esteban, A et al. (2019). “Estimation of Time-Varying Ankle Joint Stiffness Under Dynamic Conditions via System Identification Techniques.” In: *41st EMB Conference (Submitted)*.

Ogawa, Tetsuya et al. (2013). “Predictive control of ankle stiffness at heel contact is a key element of locomotor adaptation during split-belt treadmill walking in humans”. In: *Journal of neurophysiology* 111.4, pp. 722–732.

Oskoui, Maryam et al. (2013). “An update on the prevalence of cerebral palsy: a systematic review and meta-analysis”. In: *Developmental Medicine & Child Neurology* 55.6, pp. 509–519.

Pfeifer, Serge et al. (2012). “Model-based estimation of knee stiffness”. In: *IEEE Transactions on Biomedical Engineering* 59.9, pp. 2604–2612.

Pizzolato, Claudio et al. (2015). “CEINMS: A toolbox to investigate the influence of different neural control solutions on the prediction of muscle excitation and joint moments during dynamic motor tasks”. In: *Journal of biomechanics* 48.14, pp. 3929–3936.

Rack, Peter MH and DR Westbury (1974). “The short range stiffness of active mammalian muscle and its effect on mechanical properties”. In: *The Journal of physiology* 240.2, pp. 331–350.

Rouse, Elliott J et al. (2013). “The difference between stiffness and quasi-stiffness in the context of biomechanical modeling”. In: *IEEE Transactions on Biomedical Engineering* 60.2, pp. 562–568.

Sartori, Massimo, David G Lloyd, and Dario Farina (2016). “Neural data-driven musculoskeletal modeling for personalized neurorehabilitation technologies”. In: *IEEE transactions on biomedical engineering* 63.5, pp. 879–893.

Sartori, Massimo, Marco Maculan, et al. (2015). “Modeling and simulating the neuromuscular mechanisms regulating ankle and knee joint stiffness during human locomotion”. In: *Journal of neurophysiology* 114.4, pp. 2509–2527.

van Eesbeek, Stijn et al. (2010). “In vivo estimation of the short-range stiffness of cross-bridges from joint rotation”. In: *Journal of biomechanics* 43.13, pp. 2539–2547.

Weiss, PL, IW Hunter, and RE Kearney (1988). “Human ankle joint stiffness over the full range of muscle activation levels”. In: *Journal of biomechanics* 21.7, pp. 539–544.

Winter, David A (2009). *Biomechanics and motor control of human movement*. John Wiley & Sons.

Zajac, Felix E (1989). “Muscle and tendon: properties, models, scaling, and application to biomechanics and motor control.” In: *Critical reviews in biomedical engineering* 17.4, pp. 359–411.

Appendix A

SRS splines

To be able to derive SRS force and SRS for each muscle fiber two three-dimension b-splines for each MTU were created. The independent variables were normalized fiber stretch, normalized fiber length and activation. Normalized fiber stretch was only considered for lengthening of the muscle, so it took values from 0 to the critical fiber stretch (δ_c). Normalized fiber length was varied between 0.05 to 2 and fiber activation from 0 to 1.05. The SRS force spline was modelled by the following expression:

$$F_m^{SRS}(a,\bar{l}^m,\Delta\bar{l}^m)=\begin{cases}0 & ,if\Delta\bar{l}^m<0\\ \gamma F_m^0 a f_{act}(\bar{l}^m)\Delta\bar{l}^m & ,if0<\Delta\bar{l}^m<\delta_c\\ \gamma F_m^0 a f_{act}(\bar{l}^m)\delta_c & ,if\Delta\bar{l}^m>\delta_c\end{cases} \tag{12}$$

where $\gamma = 280$ is the short-range stiffness constant, F_m^0 is the maximal isometric muscle force, $f_{act}(\bar{l}^m))$ is the muscle force-length relation, $\bar{l}^m$ is the fiber length normalized by optimal fiber length , $\Delta\bar{l}^m$ is the normalized fiber stretch, a is the activation of the muscle fiber, and $\delta = 5.7 \cdot 10^{-3}$ is the normalized critical stretch. The active force-length relationship and the maximum isometric force were obtained from the file obtained during the subject-specific calibration of the model. The SRS spline was obtained by taking the partial derivative of the SRS force spline with respect to the normalized fiber length. In Fig. 9, both splines are represented for the Tibialis Anterior muscle for one representative subject.

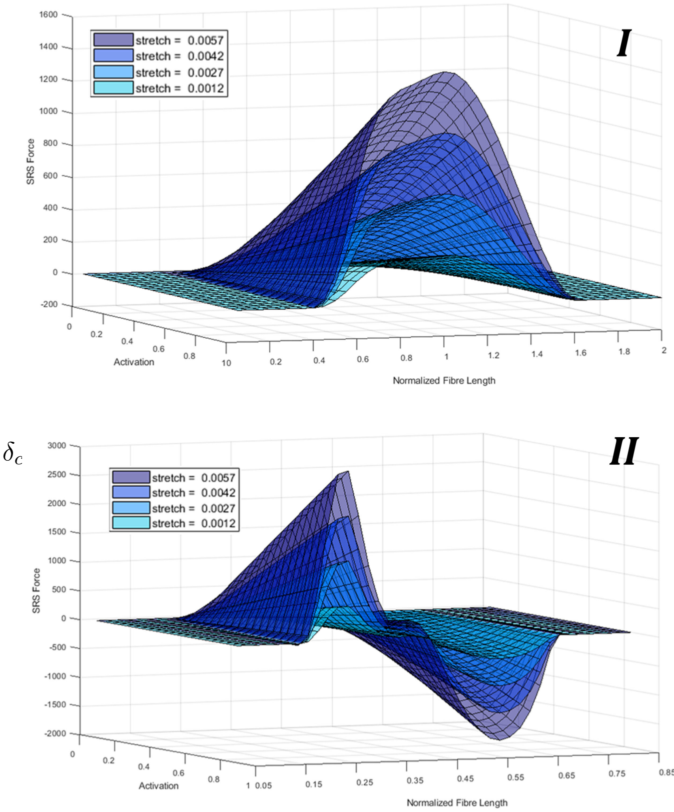

Fig. 9: I: Spline of the SRS force, computed by Eq. 5, for all possible values of fiber activation, normalized fiber length and fiber stretch. II: Spline of SRS, obtained by computing the partial derivative of the SRS force spline in terms of the normalized fiber length.

Appendix B

Optimization routine

The optimization routine was used to adjust the values of computed muscle SRS in order to account for the total fiber length amplitude throughout the entire movement. The optimized parameter was the constant G, in the function of the parameter β (Eq. 8). To create the model few parameters were designed:

- G_Max = 40 - maximum value of G.
- G_Min = 0 - minimum value of G.
- B = 200 - decay parameters of $\beta(A)$.

At each iteration, a new value of G was obtained within the solution space and the cost function was computed for that value. So, with the new value of G, the parameter $\beta(A)$ was computed for each muscle depending on the maximum length amplitude each muscle performed during the entire movement. Then muscle SRS was computed and the stiffness of each MTU was projected into the joint level to obtain joint stiffness. The cost function was computed between this estimated joint stiffness and the joint stiffness obtained by system identification, by the following function:

$$f(K)=\frac{1}{N_r}\sum_{r=1}^{\#rows}\frac{(K^j-K^{ref})^2}{VAR(K^{ref})} \tag{13}$$

At each iteration step a new cost function was computed. If the value of the cost function of the new solution was lower than the value of the cost function of the previous success, the new solution was accepted as the new success, if not the previous solution continued to be the successful one. Only integer values were acceptable for the variable G. When all of the solution space was scanned, i.e. when G took any integer value between G_Min and G_Max, the algorithm stopped. At the end, the value of G that gives rise to the lowest values of the cost function is obtained. Next you can find the pseudo-code of the algorithm:

```
G = G_0 % inital value of G
Fc = f(G) % initial cost function value
i = 1 % iterations counter
while  i < (G_Max-G_Min+1) % iteration cycle
   Gi = Perturb(G_Max, G_Min)
   Fi = f(Gi) % cost function of i^th iteration
   % Test Acceptance of new solution
   if  Fi - F > 0
      G = Gi
   end
   i = i + 1
end
```

Since the parameter $\beta(A)$ is muscle specific, but the optimization cost function is computed with the joint stiffness value, in every iteration a transition between the muscle level

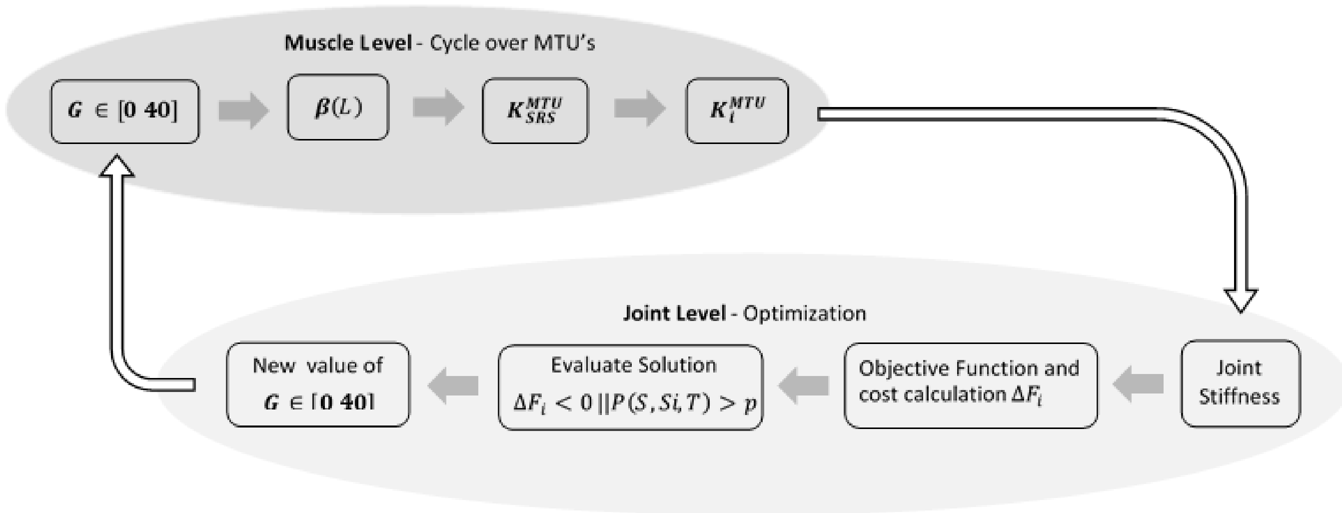

Fig. 10: Work-flow of the optimization algorithm. A value of G is chosen between the set limit values, with the new value of G a value of β is calculated for each muscle. A new SRS stiffness is computed for each muscle and it is projected at the joint level to compute joint stiffness. The estimated joint stiffness is compared with the stiffness from system identification and in case the error between the curves is smaller than with the previous value of G the solution is accepted. The algorithm end, only when G has taken all the integers values between the set limits.

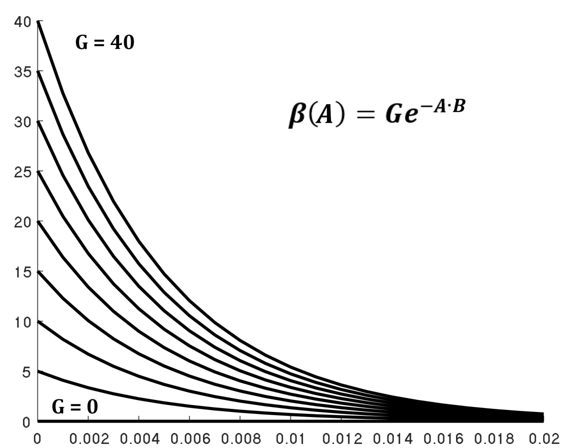

Fig. 11: Plot of the function β in function of the maximum amplitude of the muscle fibre for multiple values of G.

and the joint level is required. In Fig. 11, the function $\beta(A)$ is plotted as a function of the maximum fiber stretch throughout the whole movement cycle, A. For low values of A the function $\beta(A)$ is close to the G value, for high values of A $\beta(A)$ is close to 0. Also, $\beta(A)$ is plotted for different values of G, in which larger values of G represent large values of β and higher contribution of SRS and vice-versa. As a summary of methodology applied in this optimization algorithm the scheme in Fig. 10 was designed. The optimization was then implemented in between the blocks C and D of the EMG-driven musculoskeletal model presented in Fig. 3. However, the final joint stiffness was only computed when the optimal value of G was found for each trial.

APPENDIX C

Detection Algorithm

To detect the stretch on the muscle fibers due to the perturbation, the acceleration profile of each muscle fiber was obtained by differentiate the fiber velocity acceleration obtained in CEINMS. The detection consisted of the following steps:

1) **Design of the scanning signals (wavelets):** define the parameters of the wavelets that will be used to detect the perturbation patterns in the muscle acceleration profile.
2) **Scan signal:** Scan the signal with the designed wavelets.
3) **Compute RMSE:** Compute the RMSE between the acceleration profile and the wavelets at the different scanning points.
4) **Define Threshold:** With the values of RMSE for all the scanning points apply the muscle specific threshold to find the peaks of RMSE above that threshold.
5) **Verify Acceptance Conditions:** Verify the acceptance conditions for all the peaks detected above the previous threshold.

In this study two types of perturbations were randomly applied, a perturbation in the plantarflexion or dorsiflexion direction. So, two symmetric wavelets were designed to account for these two perturbation types. The algorithm was designed with multiple parameters that can be adjusted according to the movement characteristics:

- **Period:** In this case, as the wavelet is only composed by a single period it is equal to the duration of the signal in seconds.
- **Dephase:** when the signal starts to be scanned. This

parameter allows to avoid discontinuities due to the differentiation.

- **Scaling Factor:** This parameter is multiplied by the acceleration. For movements originating in small values of acceleration it is important to detect distinguished peak in the values of RMSE.
- **Time window:** Length of the moving step of the scanning signals.

The value of these parameters used for this study were: period = 110 ms, dephase = 200 ms, scaling factor = 1000 and time window = 4 ms (1 frame). These parameters were chosen based on the profile of the acceleration at the perturbation timing. The RMSE was mathematically manipulated, in order to obtain clear distinguished peaks on the RMSE. First the mean of the RMSE profile was removed, so the negative peaks of RMSE are the scanning points in which the wavelet was most identical with the acceleration profile. Secondly, we invert the RMSE, so now the peaks of larger similarity are the highest peaks on the RMSE. Finally, the power three of the RMSE is computed. In this way the peaks of RMSE are clearly differentiated. Besides the parameters that define the wavelets, a few more parameters were defined to control the accuracy of the detection algorithm.

- **Minimum Threshold (3):** Defines which is the minimum value of RMSE accepted in order to detect a perturbation. This allows to prevent detection of perturbations in fibers in which the acceleration was very small and perturbation have little effect on the changes in length in these muscle fibers.
- **Percentage of the threshold (40%):** The threshold which defines the peaks of RMSE was defined as a percentage of the maximum value of RMSE detected for each muscle. In this case, the threshold becomes muscle specific, since each muscle fiber has different acceleration profiles.
- **Minimum number of muscles (3):** Defines the number of parameters that a peak in RMSE needs to be detected in order to assume a perturbation.
- **Range of a perturbation (40 ms):** Minimum space in which only one perturbation can be detected. This parameters avoids that the effect of SRS is multiplied for a same instant, in the case that different muscles have perturbations on the acceleration profiles at different times.

The values used for each parameter are within brackets. The number of muscles in which a perturbation needs to be detected was chosen very conservatively. In total seven muscles were used in the model. However, two of them do not contribute for the plantar-dorsi flexion movement. So, only in 5 muscles the perturbations can be detected. Therefore we considered that the the peaks in RMSE need to be detected in 60 % of the active muscle to be accepted as a perturbation. One additional option implemented in the detection algorithm was to calculate the detection rate. A success was defined with a specific range around the real perturbation time. The successes were then divided in

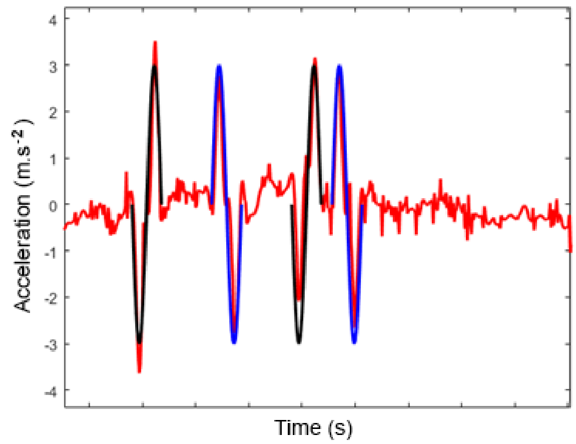

Fig. 12: Example of the acceleration profile and the two types of wavelets scanning the signal.Acceleration profile (red), plantarflexion wavelet (black) and dorsiflexion wavelet (blue).

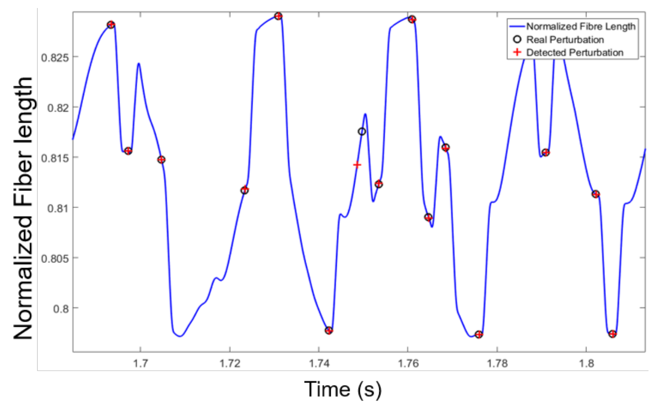

Fig. 13: Representation of the fiber length profile for the Tibialis Anterior during 4 representative cycles. Overlaid to the fiber length, the real perturbation (black circles) and the detected perturbation (red crosses) are shown. In the middle of the graph, a failed detection is shown.

three categories: exact (at the same of the real perturbation), within the first acceptance limit (Accept. Lim. 1) and within the second acceptance limit (Accept. Lim. 2). To compute these detection rates, a structure with the real times of the perturbation together with the following parameters is required:

- **Calculate Detection rate:** This is a conditional value (True of False), which does or does not trigger the calculation of the detection rates.
- **Acceptance Limit 1:** Time window of the first acceptance limit.
- **Acceptance Limit 2:** Time window of the second acceptance limit.

TABLE V: Comparison of Stiffness Estimations via EMG-driven modeling and system identification, with and without the contribution of SRS at the muscle level.

	Dynamic 0.6 Hz (Nm/rad)		Dynamic 0.3 Hz (Nm/rad)		Static (Nm/rad)	
	No SRS	SRS	No SRS	SRS	No SRS	SRS
Gas Lat	1197	169	1193	346	188	1090
Gas Med	2670	413	2644	1029	599	5691
Per Brev	2961	389	2957	1423	2690	1182
Per Long	8634	1171	7906	4979	6323	3608
Per Tert	880	155	928	386	512	2210
Soleus	9935	631	10601	3672	2255	18963
Tib Ant	4017	237	4142	691	1352	6138

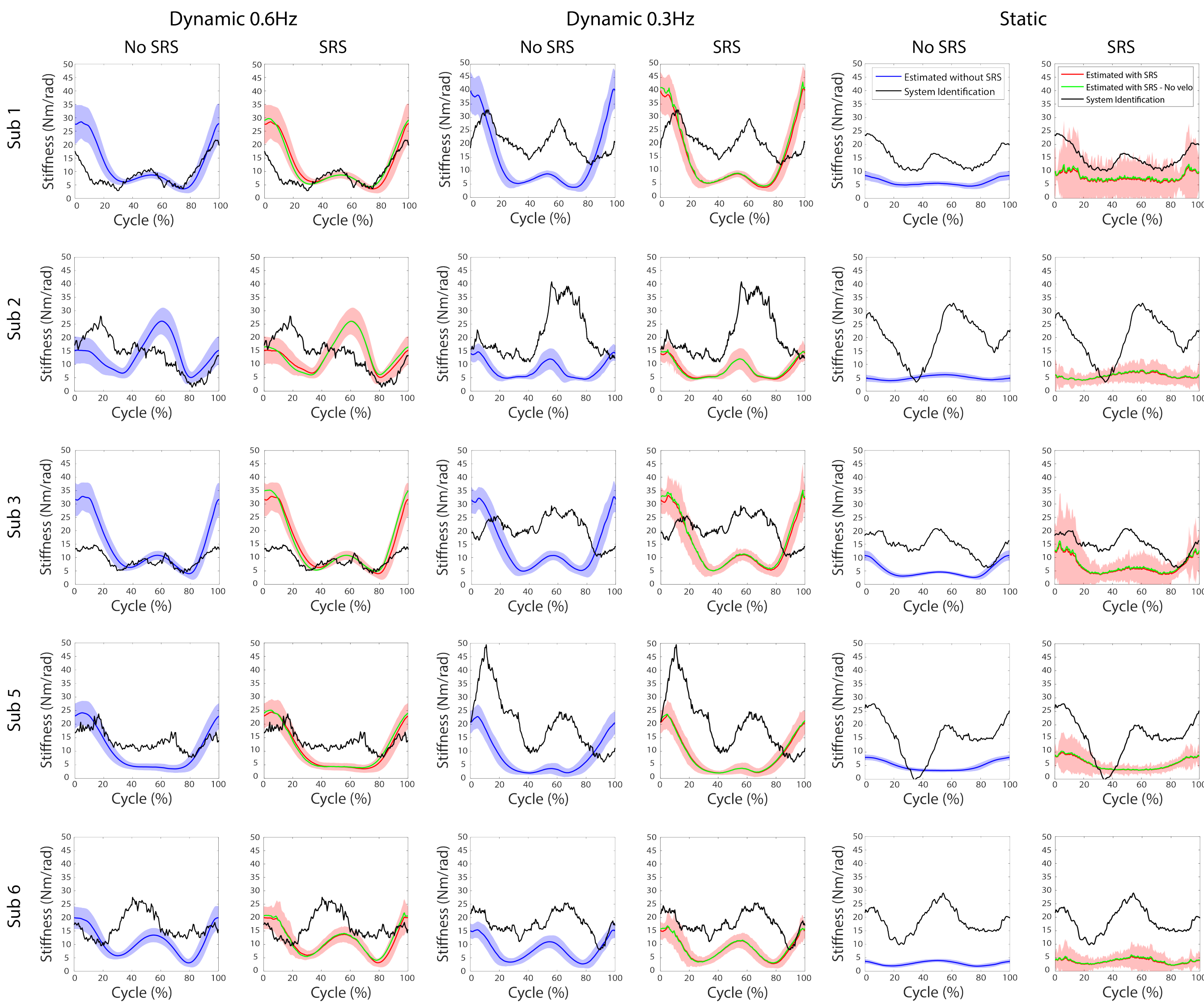

Fig. 14: Results for all subjects. Comparison between estimated stiffness and stiffness obtained in system identification techniques for the dynamic task at 0.6Hz (left), dynamic task at 0.3Hz (middle) and static task (right). The left column for each type of task contains the values of estimated stiffness without including SRS (blue) and the right column contains the values of estimated stiffness by including SRS (red) in the EMG-driven model. The green curves represent the values of estimated stiffness without accounting with the contribution of the force-velocity curve. The bold line represents the average stiffness across cycles, in each respective case by the EMG-driven model, and the shaded area corresponds to the standard deviation. The thick black line represents the average stiffness estimation via system identification.

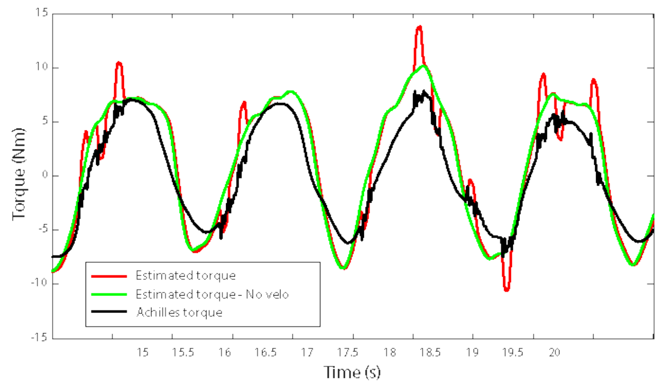

Fig. 15: Representative cycles of the Achilles torque profile, the estimated torque profile and the estimated torque profile without the force-velocity contribution. All the profiles represent the profile of torque without the inclusion of SRS.

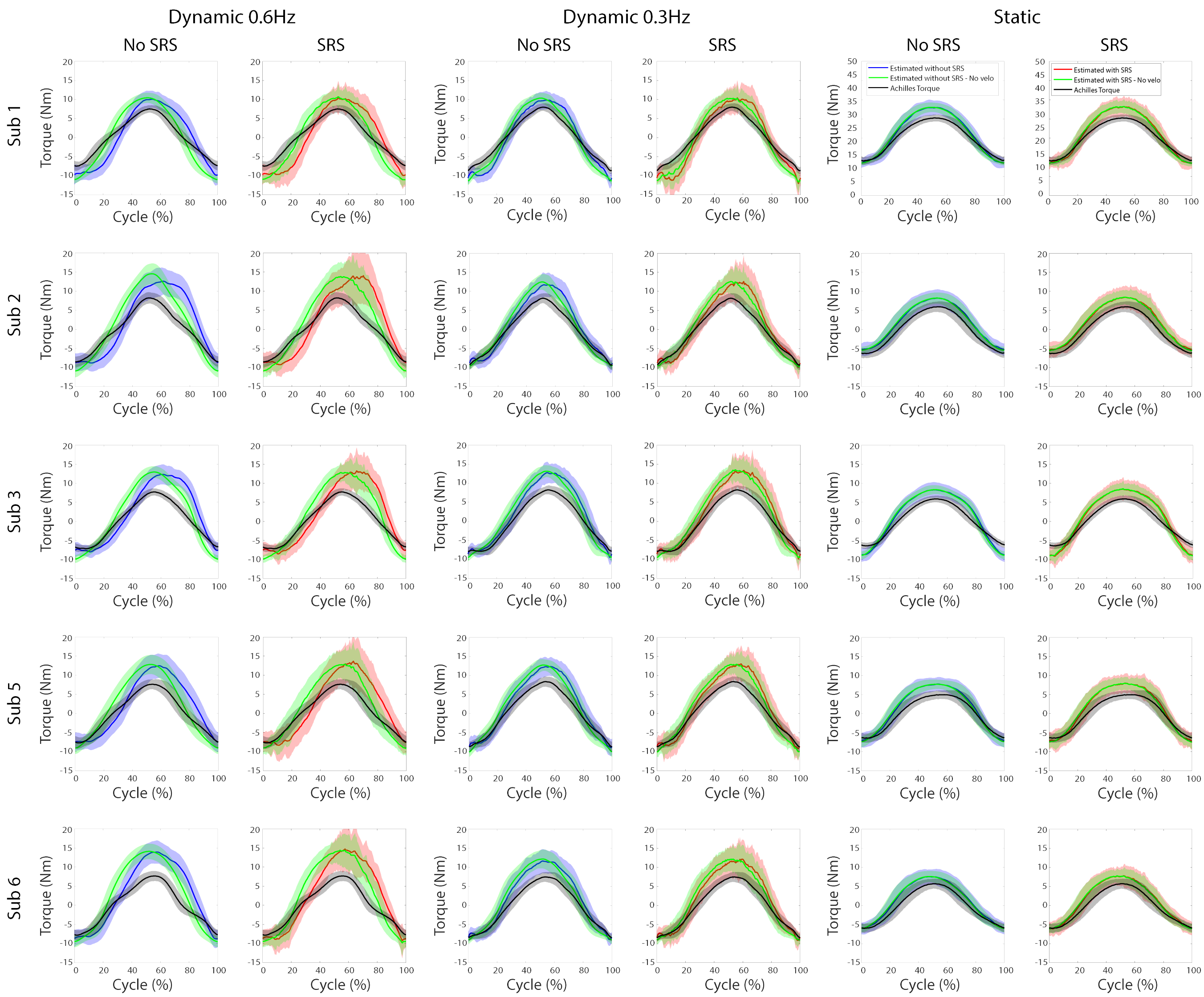

Fig. 16: Results for all subjects. Comparison between estimated torque and measured torque by the Achilles device for the dynamic task at 0.6Hz (left), dynamic task at 0.3Hz (middle) and static task (right). The left column for each type of task contains the values of estimated torque without including SRS (blue) and the right column contains the values of estimated torque by including SRS (red) in the EMG-driven model. The green curves represent the values of estimated torque without accounting with the contribution of the force-velocity curve. The black curve represents the measured torque by the Achilles device. The bold line represents the average torque across cycles, in each respective case by the EMG-driven model, and the shaded area corresponds to the standard deviation.